Inferring Progressive Disconnection in Alzheimer's Disease with Probabilistic Boolean Networks*

*Note: Sub-titles are not captured for https://ieeexplore.ieee.org and should not be used

1st Zhonglin Liu
Department of Mathematics
The University of Hong Kong
Hong Kong SAR
u3597461@connect.hku.hk

2nd Louxin Zhang
Department of Mathematics
National University of Singapore
Singapore
matzlx@nus.edu.sg

***Abstract*—Alzheimer's disease (AD) is increasingly understood as a disconnection syndrome, yet quantifying the directed influence between brain regions remains a challenge. While Probabilistic Boolean Networks (PBNs) have shown promise in modeling brain dynamics, their application to AD is largely unexplored. This study introduces a novel PBN framework to infer and analyze effective brain connectivity from fMRI data across a three-group cohort: Normal Controls (n=21), Mild Cognitive Impairment (MCI, n=28), and AD (n=10). Our robust statistical analysis identified five significant connections, all exhibiting a linear decrease in influence across the disease spectrum. The principal finding is a progressive failure of pathways from the Default Mode Network (DMN) to the Medial Temporal Lobe (MTL), quantifying a key pathophysiological mechanism of AD. These results demonstrate that the PBN framework is a powerful tool for modeling the network-level dynamics of neurodegeneration.**

***Index Terms*—Alzheimer's Disease, Brain connectivity, functional magnetic reso- nance imaging (fMRI), group analysis, probabilistic Boolean network (PBN).**

I. Introduction

Alzheimer's disease (AD) is a devastating neurodegenerative disorder characterized by progressive cognitive decline, primarily affecting memory. The modern understanding of AD has shifted from a focus on isolated regional pathology to a network-based perspective, viewing the disease as a "disconnection syndrome" where symptoms arise from disrupted communication between large-scale brain networks. Functional Magnetic Resonance Imaging (fMRI) has become an indispensable tool for investigating these network alterations *in vivo*, allowing us to measure the functional interplay between distinct brain regions. A critical goal in this field is to move beyond simple correlations and model the directed influence, or *effective connectivity*, that one brain region exerts over another.

Various computational models have been developed to infer effective connectivity from fMRI time series. Dynamic Bayesian Networks (DBNs) have emerged as a powerful statistical tool for this purpose, capable of modeling the temporal, probabilistic dependencies between brain regions. An extension of DBNs, the Probabilistic Boolean Network (PBN), offers a compelling alternative framework particularly suited for the non-linear, switch-like dynamics often assumed in block-design fMRI experiments [1]. By binarizing the fMRI signal into "on" and "off" states, PBNs can efficiently model complex logical relationships while retaining a stochastic nature. This methodology has been successfully applied to infer connectivity changes in Parkinson's disease, demonstrating its potential for clinical neuroscience [2].

Despite its successful application in other neurodegenerative disorders, the utility of the PBN framework for characterizing the progressive network failure in Alzheimer's disease has not been fully explored. This study aims to fill that gap. We present a comprehensive pipeline that applies a novel PBN inference method to fMRI data from a large cohort spanning the AD continuum: healthy Normal Controls (NC), individuals with Mild Cognitive Impairment (MCI), and patients with diagnosed AD. We hypothesize that this approach can robustly detect and quantify the gradual degradation of specific neural pathways. In this paper, we first detail our complete methodology, from fMRI preprocessing to a rigorous group statistical analysis. We then present our key findings, which reveal a systematic and linear decline in connectivity between the Default Mode and Medial Temporal Lobe networks, providing a specific, network-level mechanism for the cognitive symptoms of AD.

II. Methods

This section details the construction of a framework for inferring brain connectivity, building upon the PBN methodology proposed by Ma et al. [3]. The primary objective of this framework is to infer and quantify the functional connections between predefined Regions of Interest (ROIs) from fMRI data. This approach not only elucidates the underlying mechanisms of neural activity but also facilitates an intuitive visualization of the resulting network topologies. The methodology is implemented as a three-stage pipeline: (1) preprocessing of fMRI data, (2) inference of subject-specific PBNs, and (3) group-level statistical analysis.

Identify applicable funding agency here. If none, delete this.

A. Preprocessing of fMRI Data

Functional and anatomical data were preprocessed using **fMRIPrep 25.1.1** [4], a comprehensive neuroimaging pipeline based on Nipype 1.8.6 [5]. The T1-weighted (T1w) image was corrected for intensity non-uniformity (INU) with *N4BiasFieldCorrection* [6], and its brain was extracted using *antsBrainExtraction.sh* with the **OASIS30ANTs** template. The cortical surface was reconstructed using *recon-all* from **FreeSurfer v7.3.2** [7]. Following this, the T1w-based brain mask was refined using a custom workflow to reconcile the ANTs and FreeSurfer outputs. The T1w reference was then spatially normalized to the `MNI152NLin2009cAsym` template [8] through nonlinear registration with *antsRegistration* [9]. Brain tissue segmentation into cerebrospinal fluid (CSF), white-matter (WM), and gray-matter (GM) was performed on the brain-extracted T1w using *fast* (FSL 6.0.7.1).

The Blood-Oxygen-Level-Dependent(BOLD) data underwent several preprocessing steps. First, a reference volume was generated, and susceptibility distortion correction (SDC) was performed using a fieldmap-less, SyN-based approach, which estimates the distortion field from the subject's T1w anatomical reference. The BOLD series was then slice-time corrected using *3dTshift* from AFNI [10]and motion-corrected using *mcflirt* (FSL 6.0.7.1). The motion-corrected data were subsequently co-registered to the subject's T1w reference image using boundary-based registration (BBR) with 6 degrees of freedom, as implemented in FreeSurfer. Finally, the motion-correcting transforms, BOLD-to-T1w transform, and T1w-to-template warp were concatenated and applied in a single interpolation step to resample the BOLD series into standard space.

B. ROI definition and extraction

To investigate functional connectivity alterations in Alzheimer's Disease (AD), we defined 18 regions of interest (ROIs) based on the Automated Anatomical Labeling 3 (AAL3) atlas [11]. These ROIs were selected as key nodes within four large-scale brain networks known to be highly vulnerable to AD pathology. The Default Mode Network (DMN), critical for episodic memory, is a primary site of early amyloid-β deposition. The Executive Control Network (ECN) is crucial for higher-order cognitive functions that are progressively impaired in AD. The Salience Network (SN) mediates cognitive control, and its dysfunction contributes to attentional deficits. Finally, the Medial Temporal Lobe (MTL) network is foundational for memory and among the first to exhibit severe atrophy. Our selection comprised the bilateral Precuneus, Angular Gyrus, and Medial Orbital Frontal Gyrus for the DMN; the Superior Frontal and Superior Parietal Gyri for the ECN; the Insula and Supplementary Motor Area for the SN; and the Hippocampus and Parahippocampal Gyrus for the MTL.

The extraction process was implemented using Statistical Parametric Mapping 12 (SPM12). For each of the 18 ROIs, we first unify the repetition time (TR) to be 0.61, then a binary mask was generated from the AAL3 atlas in standard MNI space. These masks were then resampled into each participant's native functional space using nearest-neighbor interpolation to preserve their discrete anatomical boundaries. The mean BOLD signal time series was subsequently extracted from all voxels within each resampled ROI.

C. fMRI Time Series Denoising and Binarization

Following the extraction of regional mean time series, the data for each subject were further processed to generate a binary time series suitable for PBN analysis. This crucial stage consists of two sequential steps: denoising and binarization.

First, to improve the signal-to-noise ratio, the continuous BOLD signal from each of the 18 ROIs was denoised. This process included two standard procedures to remove non-neuronal noise. Guided by the work of Ma et al. [2], we applied a linear detrending operation to each time series to correct for low-frequency scanner drift. Subsequently, a bandpass filter (0.01-0.1 Hz) was applied to isolate the frequency band most associated with spontaneous neural activity and further attenuate physiological noise.

The core of this final processing stage was the binarization of the denoised time series. While simple thresholding methods (e.g., using the median) are computationally trivial, they ignore the inherent temporal dependence of the fMRI signal. A brain state at a given time point is highly predictive of its state at the next. To account for this temporal structure, we adapted the use of a Hidden Markov Model (HMM) [12] for binarization, an approach inspired by its successful application in task-based fMRI by Ma et al. [2]. However, their method leveraged the known timing of the experimental paradigm to inform the model's state transitions. As our study utilizes resting-state fMRI, which lacks an external task structure, we developed a fully data-driven, iterative HMM approach. An HMM is ideally suited for this task as it explicitly models a system with unobserved ("hidden") states—in our case, 'low' and 'high' neural activity—that evolve probabilistically over time.

Mathematically, an HMM is defined by the tuple $\lambda = (S, O, A, B, \pi)$. For our application, $S = \{s_1, s_2\}$ represents the two hidden states ('low', 'high'), and $O = (o_1, o_2, ..., o_T)$ is the sequence of observations, corresponding to the denoised BOLD signal at each time point t. The dynamics are governed by the state transition probability matrix, $A = \{a_{ij}\}$, where $a_{ij} = P(q_t = s_j | q_{t-1} = s_i)$, which we initialized with a high probability of remaining in the same state ($a_{ii} = 0.85$) and a lower probability of switching states ($a_{ij} = 0.15$ for $i \neq j$). The observation probability distribution, $B = \{b_j(o_t)\}$, defines the probability of observing a particular BOLD signal value given a hidden state. We model this as a Gaussian distribution:

$$b_j(o_t) = \mathcal{N}(o_t | \mu_j, \sigma_j^2) \tag{1}$$

where μ_j and σ_j^2 are the mean and variance of state s_j. The initial state distribution, $\pi = \{\pi_i\}$, was set to be uniform ($\pi_i = 0.5$).

Our implementation follows a robust, multi-step process for each ROI's time series. The process begins with a parameter

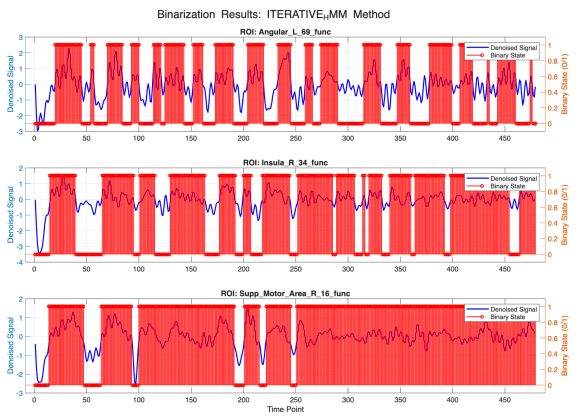

Fig. 1. Example output of the iterative HMM binarization process for three ROIs from a representative subject. The denoised BOLD signal (blue line) is shown with the corresponding inferred binary state sequence (red stems), where 1 represents a 'high' activity state and 0 represents a 'low' activity state.

initialization step where initial estimates for the two hidden states are established. To achieve this, the K-Means clustering algorithm (k=2) is applied to the denoised time series, partitioning the data points into two clusters. The means and standard deviations of these two clusters then serve as the initial estimates for the 'low' and 'high' activity states of the HMM, providing a strong, data-driven starting point for the model. Following initialization, the model is iteratively refined over three cycles to better fit the data. Within each cycle, state inference is first performed using the Viterbi algorithm [13], which finds the most probable sequence of hidden states $Q^* = \{q_1^*, ..., q_T^*\}$ that maximizes $P(O, Q|\lambda)$. Subsequently, a parameter re-estimation step recalculates the state parameters (μ_j, σ_j^2) based on this new Viterbi-derived sequence. This iterative process allows the model to converge towards a more accurate and self-consistent representation of the underlying brain states.

Finally, to ensure temporal stability and remove spurious, physiologically unlikely fluctuations, a temporal post-processing step is performed. In this last step, any state persisting for less than a predefined minimum duration (3 TRs) is merged with its neighboring state. This ensures that the final binary sequence reflects more stable periods of activation or deactivation. This iterative HMM procedure yields a robust and plausible binary time series for each ROI, as illustrated for several exemplary regions in Fig. 1, which serves as the direct input for the PBN inference pipeline.

III. Probabilistic Boolean Network Modeling

A. Theoretical Framework

Probabilistic Boolean Networks (PBNs) represent a significant advancement over traditional Boolean Networks (BNs) by incorporating stochastic properties to model complex interactions among different nodes within a system. A Boolean Network consists of a set of nodes $V = \{v_1, v_2, \ldots, v_n\}$ and a corresponding list of Boolean functions $F = \{f_1, f_2, \ldots, f_n\}$, where each Boolean function f_i is defined as a combination of logical gates (AND, OR, NOT) that regulate the connections among nodes. In this deterministic framework, each node exhibits switch-like behavior, transitioning between on and off states in the temporal dimension, with the activity of each node being governed by parent nodes through a single, fixed Boolean function. Values of nodes are synchronously updated by corresponding functions based on the current state of parent nodes, which serve as input variables to these functions.

The fundamental limitation of Boolean Networks lies in their deterministic rigidity. The temporal evolution of the entire system is completely determined by the initial state, with the system following a static transition mechanism regulated by binary functions and ultimately converging to an attractor state from which it cannot move. All possible states that converge to the same attractor state are grouped into the basin of that attractor, forming distinct basins of attraction.

To address these limitations, Shmulevich et al. proposed Probabilistic Boolean Networks, which accommodate multiple Boolean functions for each node, thereby providing substantially greater modeling flexibility [1]. The key distinction between PBNs and BNs lies in the probabilistic selection mechanism: while a BN employs a single, fixed Boolean function for each node, a PBN maintains a set of Boolean functions known as predictors for each node. The fundamental recurrence relation that governs PBN dynamics is expressed as:

$$F = \{f_j^i\}, \quad j = 1, \ldots, m, \quad \Pr(x_i(t+1) = f_j^i(t)) = p_j^i \tag{2}$$

where m is the number of predictors for node x_i, f_j^i represents the j-th predictor function for node i, and p_j^i denotes the probability of selecting predictor j at each transition, with the constraint $\sum_{j=1}^{m} p_j^i = 1$. This fundamental equation captures the essence of PBN stochasticity, where at each time step, one predictor is probabilistically selected to update the target node's state according to its associated probability.

To illustrate the conceptual difference, consider extending a three-node BN example to a PBN framework. In the original BN, node v_1 might be governed by a single Boolean function $f_1(v_2, v_3) = v_2 \wedge \neg v_3$. In the corresponding PBN, node v_1 could have multiple predictors: $f_1^{(1)}(v_2, v_3) = v_2 \wedge \neg v_3$ with probability $p_1^1 = 0.6$ and $f_1^{(2)}(v_2, v_3) = v_2 \vee v_3$ with probability $p_2^1 = 0.4$. At each time step, the system probabilistically selects between these two functions according to Equation (4) to determine the next state of v_1, introducing stochastic variability that captures the inherent uncertainty in biological systems.

The dynamic behavior of a PBN is characterized by a Markov chain whose transition matrix is defined by all possible Boolean functions and their corresponding probabilities. This probabilistic framework enables the system to exhibit more realistic behaviors compared to the rigid deterministic dynamics of traditional BNs. The long-run asymptotic

behavior of the PBN is of particular interest, specifically whether there exists a steady-state distribution that the system approaches regardless of its initial distribution. The system's reducibility properties determine whether it possesses single or multiple stationary distributions. An irreducible PBN, characterized by a communicating state space where any state can potentially be reached from any other state, possesses a unique stationary distribution. In contrast, a reducible PBN contains irreducible sets of states, with each set maintaining its own unique stationary distribution.

The steady-state behavior can be formally analyzed through the stationary distribution π, defined such that the probability of the system being in state i at any time t equals π_i when the initial distribution is π. A PBN achieves a steady-state distribution if and only if it is both irreducible and aperiodic (ergodic), satisfying the condition:

$$\lim_{t\to\infty} P_{ij}^{(t)} = \pi_j \tag{3}$$

where $P_{ij}^{(t)}$ represents the t-time transition probability from state i to state j. This probabilistic framework allows PBNs to capture the stochastic nature of biological networks while maintaining the interpretability and computational efficiency of Boolean logic.

B. Learning of PBN

The inference of network models from fMRI time series is an inherently ill-posed problem, as the number of potential interactions far exceeds the number of available time points. Methods that rely solely on time-series data are therefore susceptible to overfitting and may produce biologically implausible network structures. To overcome this challenge, we developed a multi-stage inference pipeline inspired by recent structure-aware methodologies like SAILOR [14]. Our framework is designed to systematically determine the optimal set of predictive Boolean functions for each node by synergistically integrating data-driven evidence from fMRI time series with neurobiological priors from established reference networks.

The pipeline first requires two primary types of input data for each subject: the subject-specific fMRI data (both continuous denoised BOLD and its binarized version) and a set of N=10 external reference networks derived from population-level connectivity studies. These reference networks, represented as 18×18 binary adjacency matrices, provide a crucial neurobiological prior that regularizes the model and reduces the likelihood of spurious connections.

The learning process then begins with the construction of a single hybrid influence matrix, W_{hybrid}, that balances subject-specific dynamics with this general anatomical knowledge. To achieve this, the N reference adjacency matrices are first averaged to form a probabilistic consensus matrix, A_{con}. Each entry in A_{con} represents the probability of a connection based on its prevalence across the reference atlases. Concurrently, for each subject, the continuous BOLD time series is analyzed using the `dynGENIE3` algorithm to produce an 18×18 data-driven influence matrix, W_{dyn}. These two sources of information are subsequently combined into the final hybrid matrix using a weighted linear combination:

$$W_{\text{hybrid}} = (\alpha \cdot W_{\text{dyn,norm}}) + ((1-\alpha) \cdot A_{\text{con}}) \tag{4}$$

where $W_{\text{dyn,norm}}$ is the W_{dyn} matrix scaled to a [0, 1] range, and α is the `HYBRID_ALPHA` parameter (set to 0.7).

Next, to manage the immense search space of potential predictors, a two-step pruning strategy is employed. For each of the 18 ROIs, the W_{hybrid} matrix is used to identify the `TOP_N_REGULATORS` (set to 10 for computational efficiency) with the highest influence on that target node. From this focused subset of likely parent nodes, we then generate all possible combinations of regulators, with the size of each combination ranging from 1 to a `MAX_INPUTS` constraint of 6. This combinatorial process yields a comprehensive yet manageable set of candidate predictor functions to be evaluated.

Following the search, for each candidate combination of parent nodes, the most parsimonious Boolean rule describing the relationship is inferred using the Quine-McCluskey algorithm on the subject's binarized time series data. The "goodness-of-fit" for each inferred rule is then evaluated by calculating its Coefficient of Determination (COD). The COD measures the proportional reduction in prediction error achieved by the Boolean function compared to a simple constant estimator (the mean of the target node's time series). It is defined as:

$$\text{COD} = 1 - \frac{\sum_{t=1}^{T-1}(x_i(t+1) - f_k^i(x(t)))^2}{\sum_{t=1}^{T-1}(x_i(t+1) - \bar{x}_i)^2} \tag{5}$$

where $x_i(t+1)$ is the observed state of the target node i at time $t+1$, $f_k^i(x(t))$ is the state predicted by the Boolean function, and $\bar{x}_i$ is the mean state of the target node. A higher COD score indicates superior predictive power.

Finally, after all candidate functions have been inferred and scored, they are ranked by their COD values. For each of the 18 ROIs, the top `NUM_PREDICTORS` (set to 4) with the highest COD scores are selected as the final set of predictors for that node. To assign a probability to each of these selected functions, a `softmax` function is applied to their corresponding COD scores. This normalization step converts the fitness scores into a true probability distribution $\{p_k^i\}$ for each node i. The probability for the k-th predictor of node i is given by:

$$p_k^i = \frac{\exp(\text{COD}_k^i)}{\sum_{j=1}^{4}\exp(\text{COD}_j^i)} \tag{6}$$

where COD_k^i is the Coefficient of Determination for the k-th selected predictor. The final output of this pipeline is a comprehensive, subject-specific PBN, fully parameterized and ready for group-level analysis.

C. Influence Matrix Calculation

Upon obtaining the set of predictors and their associated probabilities, the quantification of inter-node relationships is accomplished through influence value calculations. The influence of node v_j on node v_i, denoted as $I(v_j \to v_i)$, is defined

as the sum of influences across all predictors of v_i, weighted by their respective probabilities:

$$I(v_j \to v_i) = \sum_{k=1}^{4} p_k^i \cdot I_{f_k^i}(v_j) \tag{7}$$

where p_k^i is the probability of the k-th predictor function for node v_i, and $I_{f_k^i}(v_j)$ is the influence of v_j within that specific function. This per-predictor influence is calculated as the sensitivity of the function's output to the toggling of input v_j, averaged over all possible input states:

$$I_{f_k^i}(v_j) = \frac{1}{2^{|I_k^i|}} \sum_{x \in \{0,1\}^{|I_k^i|}} \left(f_k^i(x) \oplus f_k^i(x^j) \right) \tag{8}$$

where $|I_k^i|$ is the number of inputs to function f_k^i, x^j represents the input vector x with the value of v_j flipped, and $\oplus$ denotes the exclusive OR operation. This comprehensive calculation is applied across all 18 ROIs, resulting in an 18×18 influence matrix that serves as a weighted directed graph of the subject's brain network. An example of such a network is visualized in Fig. 2.

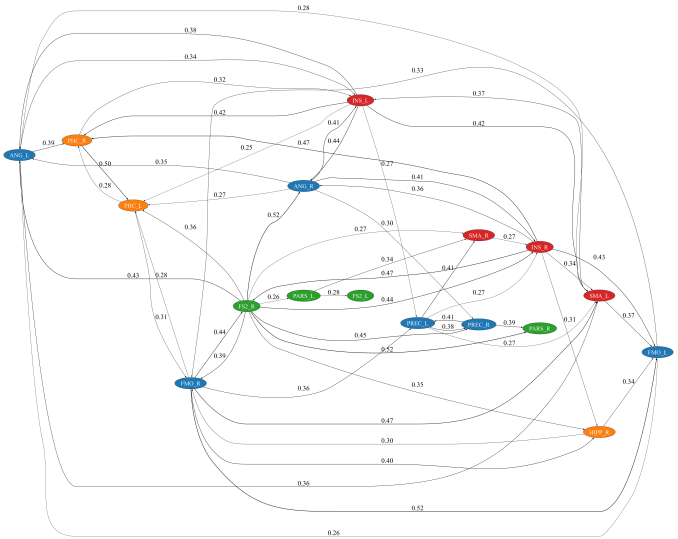

Fig. 2. An example of a learned influence network for a single subject. Edges represent the directed influence from one ROI to another, with edge thickness or color potentially representing the influence magnitude.

IV. Group Analysis and Results

To identify alterations in functional brain connectivity, we performed a group-level statistical analysis on the influence matrices derived from the Probabilistic Boolean Network (PBN) models of three distinct cohorts: Normal Control (NC, n=21), Mild Cognitive Impairment (MCI, n=28), and Alzheimer's Disease (AD, n=10). All data used in this study were obtained from the Alzheimer's Disease Neuroimaging Initiative (ADNI) database[1]. For our analysis, we specifically utilized the preprocessed resting-state fMRI series labeled as "Axial MB rsfMRI (Eyes Open)".

Participants were assigned to one of the three groups based on a comprehensive set of diagnostic and biomarker criteria. The Normal Control (NC) group consisted of cognitively normal individuals with a Mini-Mental State Examination (MMSE) score between 28-30, a Clinical Dementia Rating (CDR) Global Score of 0.0 or 0.5, and a CDR Memory score of 0.0. A key inclusion criterion for this group was a "Non-Elevated" status on amyloid Positron Emission Tomography (PET) scans, indicating no evidence of significant cortical amyloid-beta plaque deposition. The Alzheimer's Disease (AD) group included individuals with a clinical diagnosis of Dementia, characterized by MMSE scores in the range of 0-23 and significant functional and memory impairment (CDR Global Scores of 0.5-3.0; CDR Memory scores of 1.0-3.0). Critically, these participants were required to have an "Elevated" amyloid-PET status, which provides direct *in vivo* evidence of amyloid pathology, a core neuropathological hallmark of Alzheimer's disease and a key component of modern biological definitions of the disease [15]. The Mild Cognitive Impairment (MCI) group, representing a transitional stage, included participants with MMSE scores between 24-27 and a CDR Global Score of 0.5. To specifically select for an amnestic MCI subtype typical of prodromal AD, a key criterion was a score between 0.0-7.0 on the Logical Memory Delayed Recall test (LDELTOTAL). The LDELTOTAL is a sensitive measure of episodic memory, and impairment on this test is a well-established indicator of the memory deficits characteristic of early-stage AD [16].

A. Statistical Analysis

A mass-univariate statistical approach was employed. For each of the 306 possible directed connections in the 18-node network, we tested for a significant group effect. Given the unbalanced group sizes, a Levene's test for homogeneity of variances was first performed. If the assumption of equal variances was met ($p > .05$), a standard one-way Analysis of Variance (ANOVA) was used. If the assumption was violated, a Welch's ANOVA, which is robust to unequal variances, was performed [17].

To correct for the large number of simultaneous comparisons, the resulting p-values were adjusted using the Benjamini-Hochberg False Discovery Rate (FDR) procedure [18]. A connection was considered statistically significant if its FDR-corrected q-value was less than 0.05. For these significant connections, post-hoc pairwise comparisons were conducted

[1]Data used in the preparation of this article were obtained from the Alzheimer's Disease Neuroimaging Initiative (ADNI) database (adni.loni.usc.edu). The ADNI was launched in 2003 as a public-private partnership, led by Principal Investigator Michael W. Weiner, MD. The primary goal of ADNI has been to test whether serial magnetic resonance imaging (MRI), positron emission tomography (PET), other biological markers, and clinical and neuropsychological assessments can be combined to measure the progression of mild cognitive impairment (MCI) and early Alzheimer's disease (AD).

TABLE I
SIGNIFICANT CONNECTIONS SHOWING LINEAR DECREASE IN INFLUENCE

Connection	Path	q	$p_{\text{AD-N}}$	$p_{\text{AD-M}}$
PREC_R → HIPP_L	DMN→MTL	0.0017	<0.001	0.001
FMO_R → HIPP_L	DMN→MTL	0.0089	0.022	<0.001
PHC_R → PARS_L	MTL→ECN	0.0089	0.008	0.002
ANG_R → HIPP_L	DMN→MTL	0.0239	0.002	0.023
PARS_L → HIPP_R	ECN→MTL	0.0239	0.046	0.002

using either a Tukey's HSD test or a Games-Howell test, corresponding to the initial choice of ANOVA or Welch's ANOVA, respectively.

B. Significant Connectivity Changes in Alzheimer's Disease

The analysis revealed 5 connections that exhibited a statistically significant difference between the groups after FDR correction. A subsequent disease progression analysis was performed to characterize the pattern of change across the clinical stages (Normal → MCI → AD). As illustrated in Fig. 4, all 5 significant connections displayed a **Linear Decrease** pattern, where the influence value was highest in the Normal group, intermediate in the MCI group, and lowest in the AD group.

The primary finding is a profound, progressive disconnection of pathways originating from the Default Mode Network (DMN) and Executive Control Network (ECN) that target the Medial Temporal Lobe (MTL) memory system. The results are summarized in Table I and visualized in Fig. 3 and Fig. 5.

The most significant finding was the disrupted influence from the right Precuneus, a key hub of the DMN, to the left Hippocampus ($q = 0.0017$). As shown in Fig. 3a, the mean influence of this connection is clearly distinct between groups. This pattern of DMN-MTL disconnection is further substantiated by other significant pathways, with the second most significant connection also originating in the DMN (Fig. 3b).

C. Network-Level Interpretation

The overall pattern of results (Fig. 5) points to a cascade of disconnection centered on the brain's memory system. The systematic failure of three distinct DMN pathways to influence the MTL provides strong, quantifiable evidence for the DMN vulnerability hypothesis in AD [19]. The concurrent disruption of ECN-MTL circuits likely contributes to the executive function deficits that accompany memory loss in the disease. The consistent linear decrease across all significant findings, clearly visualized for the top connections in Fig. 4, suggests that our PBN framework is effectively capturing the progressive nature of the underlying neurodegenerative process.

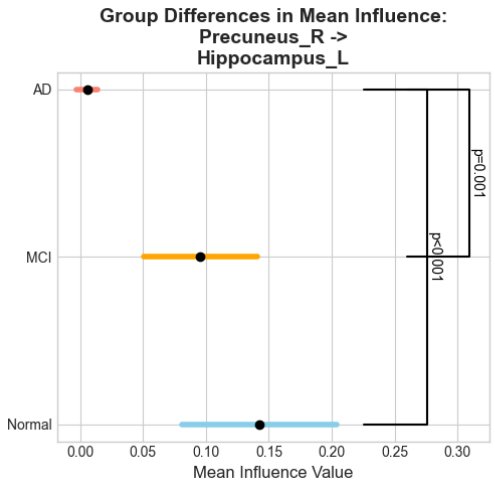

(a)

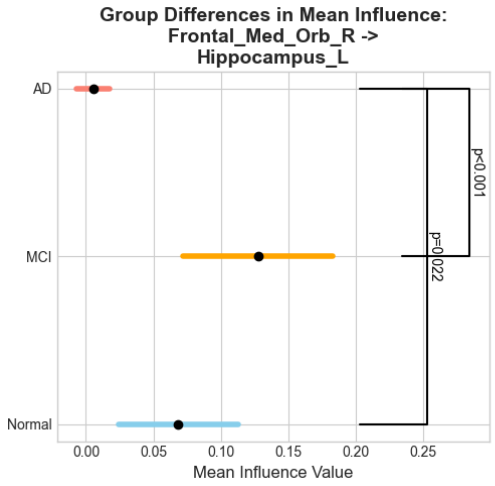

(b)

Fig. 3. Group differences in mean influence for the top two significant connections. Plots show the mean (black circle) and 95% confidence interval. Brackets indicate significant pairwise differences ($p < 0.05$). (a) The influence of the Right Precuneus (DMN) on the Left Hippocampus (MTL). (b) The influence of the Right Frontal Medial Orbital gyrus (DMN) on the Left Hippocampus (MTL).

Fig. 5. Network diagram of significant connectivity changes. Arrows indicate the 5 connections showing a significant linear decrease in influence. Nodes are colored by their respective large-scale brain networks (Blue: DMN, Orange: MTL, Green: ECN, Red: SN).

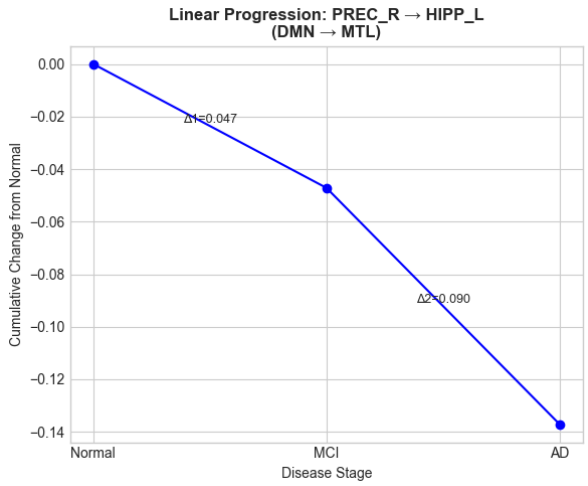

(a)

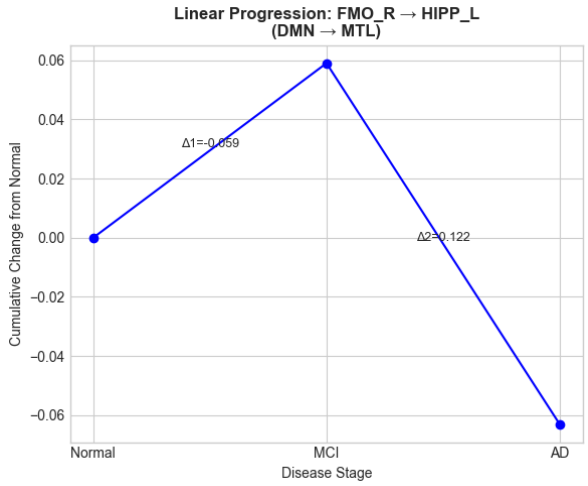

(b)

Fig. 4. Cumulative change in influence for the top two significant connections, relative to the Normal group baseline. Both connections show a linear decrease across the disease stages. Δ_1 represents the change from Normal to MCI, and Δ_2 represents the change from MCI to AD. (a) PREC_R → HIPP_L. (b) FMO_R → HIPP_L.

V. Conclusion

In this study, we introduced and validated a novel framework for inferring effective brain connectivity in Alzheimer's disease using Probabilistic Boolean Networks. By synergistically integrating data-driven fMRI dynamics with anatomical priors, our method successfully modeled the progressive disconnection across the AD spectrum, from healthy controls through Mild Cognitive Impairment to diagnosed AD. The principal finding was the identification of a specific, linear degradation in the influence exerted by the Default Mode Network onto the Medial Temporal Lobe memory system. This provides quantifiable, network-level evidence for a key pathophysiological mechanism of AD and demonstrates the utility of our PBN approach for elucidating the complex dynamics of neurodegeneration.

However, we acknowledge several limitations that offer avenues for future research. A primary limitation is the inherent information loss in the binarization of the continuous BOLD signal, a necessary step for PBN modeling. While our iterative HMM approach is sophisticated, the reduction of the signal to binary 'on' and 'off' states is a simplification of complex neural activity. Future studies could explore hybrid models that retain more of the continuous signal's richness.

Furthermore, the group analysis performed in this study employed an Individual-Structure (IS) approach, where a unique network model was learned for each subject before statistical comparison. This method excels at capturing inter-subject variability but may be less powerful for detecting subtle, common network changes compared to a Common-Structure (CS) approach, which would enforce the same network topology across subjects while allowing parameters to vary. Exploring a CS implementation of our framework is a promising direction for future work.

Despite these limitations, this paper successfully demonstrates that a structure-aware PBN framework can move beyond correlational analysis to model the directed, progressive network failures in Alzheimer's disease. The specific pathways identified here not only align with established neuropathological models but also provide novel, quantifiable targets for understanding and potentially tracking disease progression.

Acknowledgment

I would like to express my sincere gratitude to the Undergraduate Research Fellowship Programme (URFP) of the University of Hong Kong for the generous support in making this research possible. The URFP has provided me with invaluable resources and opportunities that greatly enhanced my research experience. I appreciate the guidance and mentorship offered by Professor Zhang Louxin throughout this process, which has been instrumental in the development and success of our project. The computations were performed using research computing facilities offered by Information Technology Services, the University of Hong Kong.

References

[1] I. Shmulevich, E. Dougherty, and W. Zhang, "From boolean to probabilistic boolean networks as models of genetic regulatory networks," *Proceedings of the IEEE*, vol. 90, pp. 1778 – 1792, 12 2002.

[2] Z. Ma, Z. J. Wang, and M. J. McKeown, "Probabilistic boolean network analysis of brain connectivity in parkinson's disease," *IEEE Journal of Selected Topics in Signal Processing*, vol. 2, no. 6, pp. 975–985, 2008.

[3] Y. Zhan, H. Yao, P. Wang, B. Zhou, Z. Zhang, Y. Guo, N. An, J. Ma, X. Zhang, and Y. Liu, "Network-based statistic show aberrant functional connectivity in alzheimer's disease," *IEEE Journal of Selected Topics in Signal Processing*, vol. 10, no. 7, pp. 1182–1188, 2016.

[4] O. Esteban, C. Markiewicz, R. Blair, C. Moodie, A. Isik, A. Erramuzpe, J. Kent, M. Goncalves, E. DuPre, M. Snyder, H. Oya, S. Ghosh, J. Wright, J. Durnez, R. Poldrack, and K. Gorgolewski, "fmriprep: a robust preprocessing pipeline for functional mri," *Nature Methods*, vol. 16, 01 2019.

[5] K. Gorgolewski, C. Burns, C. Madison, D. Clark, Y. Halchenko, M. Waskom, and S. Ghosh, "Nipype: A flexible, lightweight and extensible neuroimaging data processing framework in python," *Frontiers in neuroinformatics*, vol. 5, p. 13, 08 2011.

[6] N. J. Tustison, B. B. Avants, P. A. Cook, Y. Zheng, A. Egan, P. A. Yushkevich, and J. C. Gee, "N4itk: improved n3 bias correction," *IEEE transactions on medical imaging*, vol. 29, no. 6, pp. 1310–1320, 2010.

[7] A. M. Dale, B. Fischl, and M. I. Sereno, "Cortical surface-based analysis: I. segmentation and surface reconstruction," *NeuroImage*, vol. 9, no. 2, pp. 179–194, 1999. [Online]. Available: https://www.sciencedirect.com/science/article/pii/S1053811998903950

[8] V. Fonov, A. Evans, R. McKinstry, C. Almli, and D. Collins, "Unbiased nonlinear average age-appropriate brain templates from birth to adulthood," *NeuroImage*, vol. 47, p. S102, 2009, organization for Human Brain Mapping 2009 Annual Meeting. [Online]. Available: https://www.sciencedirect.com/science/article/pii/S1053811909708845

[9] B. Avants, C. Epstein, M. Grossman, and J. Gee, "Symmetric diffeomorphic image registration with cross-correlation: Evaluating automated labeling of elderly and neurodegenerative brain," *Medical Image Analysis*, vol. 12, no. 1, pp. 26–41, 2008, special Issue on The Third International Workshop on Biomedical Image Registration – WBIR 2006. [Online]. Available: https://www.sciencedirect.com/science/article/pii/S1361841507000606

[10] R. W. Cox, "Afni: Software for analysis and visualization of functional magnetic resonance neuroimages," *Computers and Biomedical Research*, vol. 29, no. 3, pp. 162–173, 1996. [Online]. Available: https://www.sciencedirect.com/science/article/pii/S0010480996900142

[11] E. T. Rolls, C.-C. Huang, C.-P. Lin, J. Feng, and M. Joliot, "Automated anatomical labelling atlas 3," *NeuroImage*, vol. 206, p. 116189, 2020. [Online]. Available: https://www.sciencedirect.com/science/article/pii/S1053811919307803

[12] L. Rabiner, "A tutorial on hidden markov models and selected applications in speech recognition," *Proceedings of the IEEE*, vol. 77, no. 2, pp. 257–286, 1989.

[13] G. Forney, "The viterbi algorithm," *Proceedings of the IEEE*, vol. 61, no. 3, pp. 268–278, 1973.

[14] Ž. Pušnik, M. Mraz, N. Zimic, and M. Moškon, "Sailor: Structure-aware inference of logic rules," *PLOS ONE*, vol. 19, no. 6, pp. 1–29, 06 2024. [Online]. Available: https://doi.org/10.1371/journal.pone.0304102

[15] C. R. Jack Jr., D. A. Bennett, K. Blennow, M. C. Carrillo, B. Dunn, S. B. Haeberlein, D. M. Holtzman, W. Jagust, F. Jessen, J. Karlawish, E. Liu, J. L. Molinuevo, T. Montine, C. Phelps, K. P. Rankin, C. C. Rowe, P. Scheltens, E. Siemers, H. M. Snyder, R. Sperling, Contributors, C. Elliott, E. Masliah, L. Ryan, and N. Silverberg, "Nia-aa research framework: Toward a biological definition of alzheimer's disease," *Alzheimer's & Dementia*, vol. 14, no. 4, pp. 535–562, 2018. [Online]. Available: https://alz-journals.onlinelibrary.wiley.com/doi/abs/10.1016/j.jalz.2018.02.018

[16] S. Weintraub, D. Salmon, N. Mercaldo, S. Ferris, N. Graff-Radford, H. Chui, J. Cummings, C. DeCarli, N. Foster, D. Galasko, E. Peskind, W. Dietrich, D. Beekly, W. Kukull, and J. Morris, "The alzheimer's disease centers' uniform data set (uds): The neuropsychologic test battery," *Alzheimer Disease and Associated Disorders*, vol. 23, no. 2, pp. 91–101, Apr. 2009.

[17] B. L. WELCH, "On the comparison of several mean values: An alternative approach," *Biometrika*, vol. 38, no. 3-4, pp. 330–336, 12 1951. [Online]. Available: https://doi.org/10.1093/biomet/38.3-4.330

[18] Y. Benjamini and Y. Hochberg, "Controlling the false discovery rate: A practical and powerful approach to multiple testing," *Journal of the Royal Statistical Society: Series B (Methodological)*, vol. 57, no. 1, pp. 289–300, 12 2018. [Online]. Available: https://doi.org/10.1111/j.2517-6161.1995.tb02031.x

[19] Y. Wang, S. Risacher, J. West, B. Mcdonald, T. MaGee, M. Farlow, S. Gao, D. O'Neill, and A. Saykin, "Altered default mode network connectivity in older adults with cognitive complaints and amnestic mild cognitive impairment," *Journal of Alzheimer's Disease*, vol. 35, pp. 751–760, 05 2013.